International Journal of Engineering Research and Technology. ISSN 0974-3154, Volume 12, Number 12 (2019), pp. 2452-2464

The Calculation of the Stress-Strain State of Mine Workings in the Networks of Complex Fault Lines in Planes, Generalized Planar and Volumetric Installations

G. Salgarayeva, N. Kurmanbekkyzy, N. Katayev, G. Askarova, S. Omarova

Department of Informatics and Applied Mathematics, Kazakh State Women's Teacher Training University, Ayteke-bi St. 99 – 050026, Almaty, Kazakhstan.

Abstract:

Mountain ranges are affected not only by physical and chemical processes but also by tectonic forces. This results in rock discontinuity, including the appearance of various small cracks and fissures that grow into large fault lines. The mechanical and mathematical models typically consider small fissures as parallel and periodic (or doubly periodic) and take into account their effect on the physical-mechanical properties of the mass. Local fissures are assessed using several parameters, and their length and depth can stretch for many kilometers, potentially breaking the Earth's surface. Geologic fissures are measured on a global scale and, riving the whole layer of the lithosphere; they reach the Earth's mantle. Some aspects of the stability of underground workings in difficult mountain ranges remain unexplored or require more comprehensive study. These include regularities of stress concentrations around the boarding gate, cross-drift, and cut-offs, which we address here using new mechanical models that also take into account the properties of the isotropic, transverse, and inclined anisotropic layers. However, in nature, mountain ranges are composed of multiple layers. Therefore, stress concentrations can appear at the boundaries of heterogeneous layers or in the vicinity of tectonic fissures and fault lines, even before conducting underground work. The interactions between these layers and stress concentration succoring around mine workings require further research.

Keywords - Complex Fault Line, Plane, Generalized-Plane, Volumetric Settings, Stress Concentrations.

I. INTRODUCTION

The pressure forces above mine working sarising from the geostatic field in the layers up to the Earth's surface have only been addressed using Dinnik's hypothesis [1]. Since tectonic forces are changing slowly over geological time and resources are limited, studies often fail to account for their effect. Data from multipled eposits Khibiny in Europe, and Bayzhan say and Myrgalym say in Asia shows that the values and directions of tectonic forces measured at different depths are not subject to the linear laws, as proposed in Dinnik's hypothesis [1]. Thus, it can be concluded that the initial mechanical stress state of the integral mass will be diverse at different depths under the action of tectonic forces. Therefore, the regularities of the stress concentration distribution in the vicinity of mine workings occurring under its effect will be distinct (both in value and direction) from the established regularities only under the geostatic field effect. The study of such issues is further complicated by the influence of man-made explosions or moderate earth quakes. By ignoring such factors, the forecast of critical stresses around mine working might be erroneous. Also, adiabatic processes of sudden gas outbursts in the deposits, which consistently result in the loss of human life, arise from large stress concentrations.

Addressing the anisotropic mass's elasticity theory, the work of multiple authors over many decades has demonstrated that the elasticity properties of samples differ across various directions [2-4]. A sample's elasticity can be defined by the pressure on the sample's layers by parallel or perpendicular forces; however, this approach is limited to the qualitative aspect. To define the degree of anisotropic elasticity for plane problems, Lekhnitskiy proposed a method of defining parameters of anisotropy strength.

Defining the stability of underground structures depends upon finding stress-deformed conditions around it. Fotiyeva, Bulychev, Firsanov, Deev [5] and others made progress in understanding the plane stability of underground structures, whereas the Kazakh scientific school under the guidance of Aytaliyev [6], Masanov [7] and Baymakhan [8], principally addressed the plane, generalized-plane, and spatial stability of some types of workings of the anisotropic mass, such as boarding gates, cut-offs, and cross-drifts, widely spread in mining and ore deposits. In recent years, much attention has also been paid to the dynamical stability of underground structures, mechanisms of the mass's destruction in its vicinity, and accounting for the effect of gravitation and tectonic forces. Currently, there is a need to investigate the stability of underground workings in the vicinity of various geologic fissures.

When FEMs (finite element methods) are used, the main tasks are to choose the boundaries of the investigated computational region and to define the accuracy of the calculations. There is no available computational method that can be applied to investigations of the working's stability on the geostatic field located around the geologic fault. To do this, it is necessary to define how the lengths of three parameters (OX, OY, and OZ) can be set and to substantiate their accuracy. Here, the accuracy of the calculations is confirmed by the condition of equality of the vertical stress component around the fault and the geostatic field stress γH on removal from it. The unknown quantity is defined by multivariate numerical calculations with the purpose of selecting different geometric parameters for components of

the three-dimensional field. The general plan of the new computational region is shown in Fig. 1.

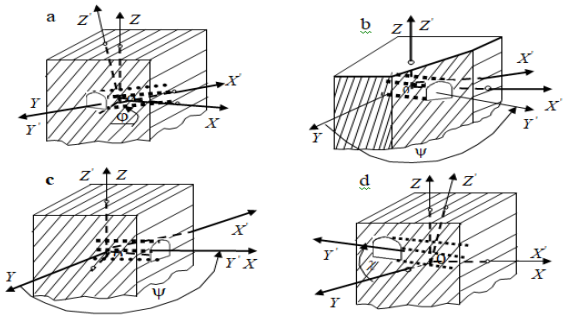

Fig. 1. Underground workings around a geologic fault in an inclined transversely isotropic mass in the case of gravity. (a) Boarding gate; (b)cross-drift; (c) inclined working; and(d) uneven relief of the Earth's surface.

Here, *a* is the boarding gate and *b* is the cross-drift. The cut-off not shown in the Fig. is between these two sections (i.e., $0 < \psi < 90^0$). Carrying out digs is shown in the Fig., where *c* is the inclined working in the inclined transversely isotropic mass, and *d* is the relief roughness (i.e., mountain peaks). The given computational region closely characterizes the mines of Kadamzhay, Tekeli, and Khaidarkent, where underground studies have measured geostatic and tectonic forces [9]. As each separate mine is characterized by a wide diversity of large and local geologic faults of the mass, filled with coarse clastic and sedimentary materials, to get a general picture, we identified that mine workings were located in two directions.

We shall further calculate the mechanic-mathematical model for the field of finite elements in the half-space, as represented in Fig. 2.

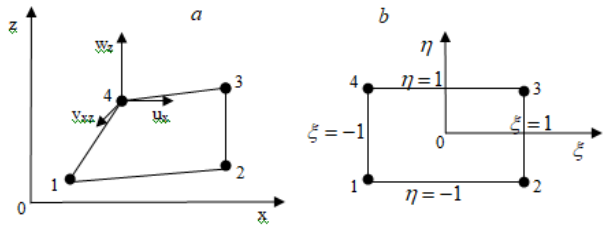

Fig. 2. The computational region of interest, including the mine working

Here, height (H) defines the depth from the Earth's surface, and $H = 0$ means the Earth's surface. The task consists in pointing lengths to the sides H, L and N. If for some chosen depth of the working in the half-space small length values are set, then solving the system of finite elements equations (by the definition of displacement, deformation, and stress components) might lead to incorrect solutions. However, even when larger values are set, thesolution might still be erroneous. Therefore, the setting of these parameters should be clearly substantiated. For example, it has been shown that, for the finite-element model, the working in the unbroken mass without taking into account the weight of boundaries should be set as the ratio $L = H = 3r$. Here r is the radius of the working's arch. However, for substantiation of boundaries in the working's computational region under the influence of gravity and tectonic forces, this condition does not work. The value of the stress component σ_z, calculated from the region of stress concentrations around the mine working, will not be equal to the value γH of Dinnik's hypothesis [1]. First, computer-based numerical calculations have been used to define the ratio of H and L for the plane case. Based on experimental calculations for cases with and without mine workings, the following condition for defining ratios was obtained:

$$L \geq 600r,$$

$$H = \frac{L}{\delta}, \quad (1)$$

$$h = \frac{H}{2},$$

$$N \geq L,$$

$$2.2 \leq \delta \leq 2.3, \; r \geq 1$$

Only such a selection of boundaries of the computational region helps obtain the value of the vertical stress component equal to γH for zones out of stress concentrations.

The calculation models thus far proposed are insufficient for investigating the stability of the geostatic field of underground workings near the geologic fault in the half-space. The accuracy of the given model is confirmed by the equality of the horizontal stress component σ_z to the geostatic field stress γH in the unbroken mass at depth H for any zone far from the geologic fault and mine working. The methods used to test the accuracy of the solved task are shownin Fig. 3.

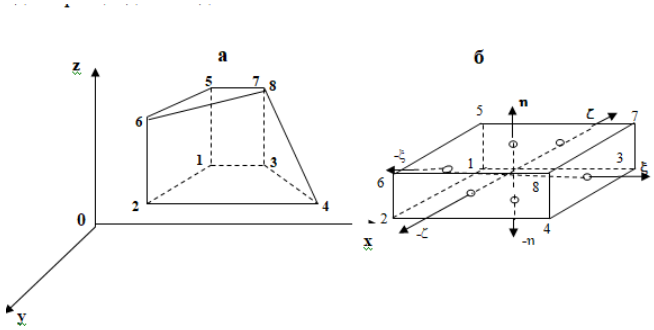

Fig. 3. The fragment of discretization by finite elements of the mass, including amine working and a geologic fault

Here, the depth H equals 300 m, and the mass's volumetric weight is $\gamma = 0.0025 MH/m^3$, so that $\gamma H = 75 MPa$. $\sigma_Z \cong \gamma H$ is required for the calculation to be considered accurate. By the results of the calculations $\sigma_Z = (74.2 - 74.6)\, MPa$ for zones with a distance of (8–10) r from the working's arch in the transverse direction and farther. Above the working's arch, at its foundation, and in the

points on the surface $\sigma_z = (0.002 - 0.01)\ MPa$ or 0.2–1%. Moreover, in other points of the working's contour, the greatest inaccuracy is 3–5%.

As can be seen from Fig. 3, in conditions of weightlessness, the substantiation of boundaries of the computational region with mine workings cut out from infinity under the condition $L = H = 3r$ is different from our condition. According to our condition, when $r = 0$ (i.e., under the absence of mine workings)the boundary conditions are defined as $L = \delta H$. The spatial task requires the third component to be $N \geq L$. Under the absence of mine workings, L is any number, $H = \frac{L}{\delta}$, and in the context of the model with mine workings $H = \frac{L}{\delta}$ but $L \geq 600r$, and the depth is $h = \frac{H}{2}$.

II. MATERIAL AND METHODS

II.I General Part

Here we use the FEM to solve three-dimensional tasks [10]. For the computational region, we developed a FEM-based system of algebraic equations, as follows:

$$[K]\{U\} = \{\gamma H\} + \{T\} + \{P\}, \quad (2)$$

where $[K]$is the stiffness matrix, $\{U\}$is the displacement vector, $\{\gamma H\}$is the vector of geostatic forces, increasing proportionally to depth *H*, $\{T\}$is the vector of tectonic forces, and $\{P\}$is the vector of relief (mountain slopes) gravity. At generalized-plane deformation, the measurement of the stiffness matrix and all vectors is equal to 3 × n. Here n is the number of nodal points of the region, modeled by finite elements. There are three stress components and three deformation components in the plane task, $\sigma_x, \sigma_z, \tau_{zx}$ and $\varepsilon_x, \varepsilon_z, \gamma_{zx}$respectively, as well as six in the spatial task $\sigma_x, \sigma_y, \sigma_z, \tau_{yz}, \tau_{zx}, \tau_{xy}, \varepsilon_x, \varepsilon_y, \varepsilon_z, \gamma_{yz}, \gamma_{zx}, \gamma_{xy}$ and five in the generalized-plane task $\sigma_x, \sigma_z, \tau_{yz}, \tau_{zx}, \tau_{xy}$, $\varepsilon_x, \varepsilon_z, \gamma_{yz}, \gamma_{zx}, \gamma_{xy}$. In all three cases, the values of isoperimetric elements are defined by the internal points of integration of every element. If the finite element dimension is relatively small, the mean values of stress components at those points are used, and when the sizes of elements are larger, the values of integral points are used. The displacement components $u, \vartheta, w$are calculated for general vertices of elements.

Now we shall set the boundary conditions for the spatial computational region of Fig. 1. The displacement components were located along the OY axis: on the ABCD plane $V = 0$; on the EFGH plane $V = 0$;along the OZ axis: on the AEHD plane $U = 0$;on the BFGC plane $U = 0$; the foundation on DHGC $W = 0$; and the Earth's surface AEFB

$$\sigma_n = 0,\ \tau_n = 0. \quad (3)$$

For solving the system of algebraic equations (2) by the defined boundary conditions, we used an iteration method. The iteration method was divided into Jacobi, Seidel, Richardson, and successive over-relaxation types. The most accurate and reliable method is the Gauss-Seidel method, using the Young's coefficient [11, 12].

For the n of the nodal points of the spatial task, a system of equations with dimensions of $3nx3n$ is formed. A peculiarity of the FEM is that the dimension of the stiffness matrix does not exceed (2) for the hexahedral element 45, and for the element in the form of a volumetric prism of the second order 81, as every point is only connected to closely located points. Proceeding from the above boundary conditions, the displacements at the point of $3*p$ equal zero and cannot be included in the system. Thus, the number of equations will be reduced from $3nx3n$ to $3*(n-p)x3*m$. Each point in the elastic spatial mass, in conjunction with the points located in the immediate neighborhood, forms a set of spatial "stars", each of which has m points. As for the system of equations (2) with dimensions of $q = n - p$, we have:

$$[K(3*q, 3*m)]\{U(3*q)\} = \{\gamma H(3*q)\} + \{T(3*q)\} + \{P(3*q)\} \quad (4)$$

If we solve the last set of equations using the Gauss method, we will perform $3*q\ x\ 3*m$ actions for the upper triangular matrix and $3*q\ x\ 3*m$ actions for back substitution. In the context of the iteration method, $3*q\ x\ 3*m$ actions are performed for each iteration only once, and it only remains to multiply a vector by a matrix. As a result, according to the Gauss method, the number of actions is proportional to t^3, and according to the iteration method, t^2 actions are carried out. Thus, it follows that to solve spatial problems with tens of thousands of indeterminates, the iteration method is more efficient. Furthermore, the errors that occur due to rounding sare spontaneously adjusted with respect to the predetermined accuracy $\bar{\varepsilon} = 10^{-\bar{c}}$. According to the Jacobi method, in order for the selection of the displacement component in the n-line (4) of the system of equations to be transformed into the iterative form, the following algorithm should be used:

$$u_n = K_{nn}^{-1}\{F_n - \sum_{i=1}^{n-1} K_{ni}u_i - \sum_{i=n+1}^{N} K_{ni}u_i\}. \quad (5)$$

Let us determine the Gauss-Zeidel algorithm:

$$u_n^m = K_{nn}^{-1}\{F_n - \sum_{i=1}^{n-1} K_{ni}u_i^m - \sum_{i=n+1}^{N} K_{ni}u_i^{m-1}\}. \quad (6)$$

The algorithm of the successive over-relaxation method with acceleration factor $\overline{\beta}$ is given in the following form:

$$u_n^{\overline{m}} = u_n^{\overline{m}-1} + \beta(u_n^{m^*} - u_n^{\overline{m}-1}). \quad (7)$$

Since this method is used, let us give its brief algorithm.

Here $u_n^{m^\bullet}$ is the solution obtained from formula (6). According to Young [12], $1 < \overline{\beta} < 2$. The computational tests have shown that, for elasticity problems, $\overline{\beta} = 1.88$ is the most appropriate value. Other researchers have proposed a value of $1.85 < \overline{\beta} < 1.90$ [7, 6, 8];. $\{F\}$ from the above equations (5) and (6) is the sum of forces from the right side of the system of equations (2), $\{F\} = \{\gamma H\} + \{T\} + \{P\}$, while $\overline{m}$ and $m^\bullet$ are the iteration numbers with the values of the displacements specific for pre-diagonal and off-diagonal elements of the n line and 3^*m column of equations. To reduce computer random access memory and time required for the calculations, using symmetric and band properties towards the diagonal of the stiffness matrix, iteration is applied only to $3^*m/2$ pre-diagonal elements. Fig. 3 through k presents m of the lengths of numbers that are not equal to zero around the diagonal of the n line (circled with two slanting lines).

$$[K] = \begin{bmatrix} k & 0 & 0 & 0 & 0 & 0 & 0 & 0 \\ 0 & kkk & 0 & 0 & 0 & 0 & 0 & 0 \\ 0 & kkkk & 0 & 0 & 0 & 0 & 0 & 0 \\ 0 & 0 & kkkk & 0 & 0 & 0 & 0 & 0 \\ 0 & 0 & 0 & kkkkk & 0 & 0 & 0 & 0 \\ 0 & 0 & 0 & 0 & kkkkk & 0 & 0 & 0 \\ 0 & 0 & 0 & 0 & 0 & kkkkk & 0 & 0 \\ 0 & 0 & 0 & 0 & 0 & 0 & kkk & 0 \\ 0 & 0 & 0 & 0 & 0 & 0 & 0 & k \end{bmatrix} \quad (8)$$

For the remaining numbers that equal 0, iterations are not performed (i.e., they are not taken into account). The k, kkk, $kkkk$ in proximity with the diagonal denote the set of "stars" mentioned above. The dotted line is the line of symmetry on the diagonal, and the number of elements before it equals $3^*m/2$. Drawing the stiffness matrix in such a way is one of the basic properties of the FEM.

II.II Computational Regions Compiling for Multivariate Calculations

Fig. 4 shows the computational region of the task in most common view. To make research area sin Fig. 1 and Fig. 2 clearer, let us give the image of the cross sections parallel to ABCD on the ZOX plane, which is perpendicular to the OY axis.

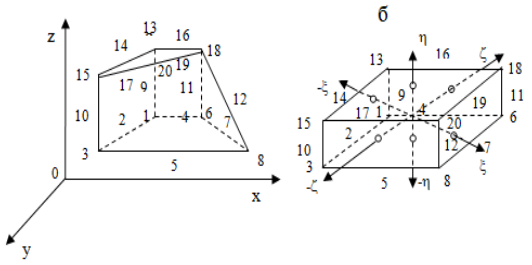

Fig. 4. The general computational region of interest, including the mine working's compression strength, passed through a complex system of tectonic faults in the dipping layer of the anisotropic mass, taking into account ground mountain slopes and the effect of geostatic, tectonic and seismic forces. (1) Tectonic faults;(2) geostatic forces;(3) tectonic forces; (4) seismic forces from transient seismic waves;(5) soils and mantle; and (6) rock mass of the dipping-layered anisotropic structure

In Fig. 5, we give the finite element computational region of the mass with an arched mine working and a vertical fault to its right.

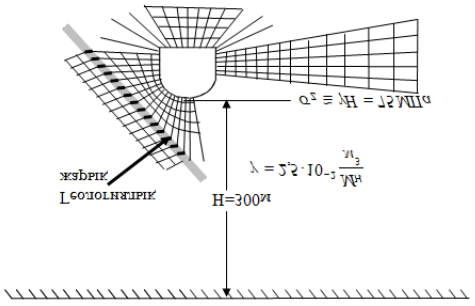

Fig. 5. The mine working around a vertical fault and the direction of the horizontal components of geostatic and tectonic forces. (1) The geologic fault; (2) the direction of the geostatic force field; and (3) the direction of the vertical component of tectonic forces

In the calculation of the stress-deformed state, the distance between the mine working and the fault will vary. The geometrical parameters H, L, and h are set according to the conditions:

$$[J]^{-1} = \frac{1}{\det[J]} \begin{bmatrix} \overline{a}_{11} & \overline{a}_{12} & \overline{a}_{13} \\ \overline{a}_{21} & \overline{a}_{22} & \overline{a}_{23} \\ \overline{a}_{31} & \overline{a}_{32} & \overline{a}_{33} \end{bmatrix} \quad (9)$$

The dimensions of the working are not indicated as they might be different. The directions of force components are indicated as follows: geostatistical components are directed downward, tectonic – from right to left. Although the geologic fault might

reach the Earth's surface, this might not happen; therefore, one variant is given.

Fig. 6 shows the computational region of the mine working an adjacent to a complex geological fault (two vertical parallel faults).

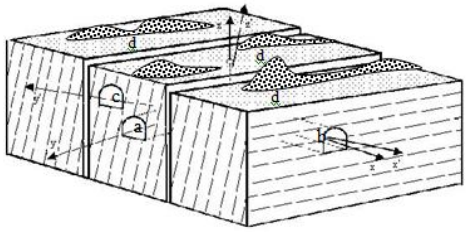

Fig. 6. The mine working driven alongside vertical faults, parallel to each other, and tectonic force directions. (1) The geologic fault; (2) the direction of the geostatic force field; and (3) the direction of the horizontal component of tectonic forces

The location of the mine working driven towards perpendicularly crossed faults is shown in Fig. 7.

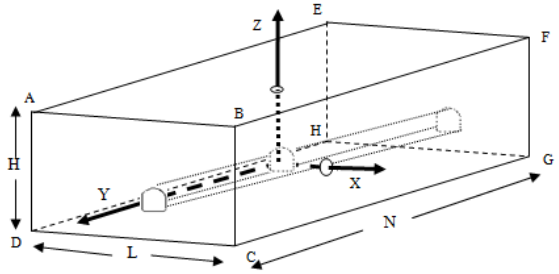

Fig. 7. The mine working driven alongside crossing faults, perpendicular to each other. (1) The geologic fault; (2) the geostatic force direction; (3) the direction of the horizontal component of tectonic forces

Finally, the variations of paths driven by the mine working alongside almost parallel horizontal and inclined faults in the hanging are shown in Fig. 8 and Fig. 9.

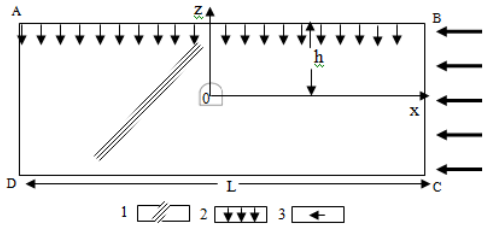

Fig. 8. The computational region of the mine working around faults (from the left top and the right bottom). (1)The geologic fault; (2) the direction of the geostatic force field; and (3) the direction of the horizontal component of tectonic forces

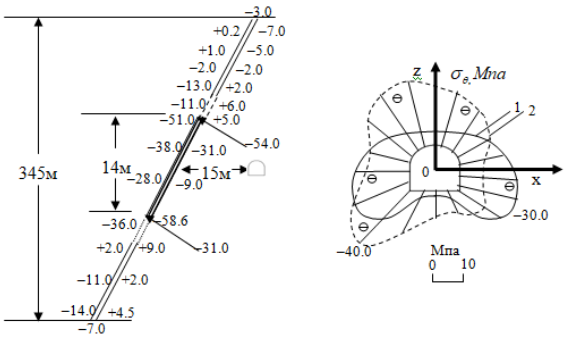

Fig. 9. The computational region of the mine working driven alongside an inclined fault. (1) The geologic fault; (2) the direction of the geostatic force field; and (3) the direction of the horizontal component of tectonic forces

III.III Algorithm development for multivariate calculations

Let us define the parameters of the forces that are included in the system of equations featuring the balanced condition of theisotropic and anisotropic mass withfaults andunderground workings:

$$[K]^e = \sum_{i,j,k} t_{i,j,k}\alpha_{i,j,k}[B]^T_{i,j,k}[D][B]_{i,j,k}\det[J]_{i,j,k} \qquad (1),$$

The formula of elastic forces on the left side of the equation includes the stiffness matrix $[K]$. In determining $[D]$, this matrix is defined by equations (10), (11), and (12):

$$[B]_{i,j} = \begin{bmatrix} \frac{\partial h_1}{\partial x} & 0 & 0 & \frac{\partial h_2}{\partial x} & 0 & 0 & \frac{\partial h_3}{\partial x} & 0 & 0 & \frac{\partial h_4}{\partial x} & 0 & 0 \\ 0 & \frac{\partial h_1}{\partial z} & 0 & 0 & \frac{\partial h_2}{\partial z} & 0 & 0 & \frac{\partial h_3}{\partial z} & 0 & 0 & \frac{\partial h_4}{\partial z} & 0 \\ 0 & 0 & \frac{\partial h_1}{\partial z} & 0 & 0 & \frac{\partial h_2}{\partial z} & 0 & 0 & \frac{\partial h_3}{\partial z} & 0 & 0 & \frac{\partial h_4}{\partial z} \\ \frac{\partial h_1}{\partial z} & \frac{\partial h_1}{\partial x} & 0 & \frac{\partial h_2}{\partial z} & \frac{\partial h_2}{\partial x} & 0 & \frac{\partial h_3}{\partial z} & \frac{\partial h_3}{\partial x} & 0 & \frac{\partial h_4}{\partial z} & \frac{\partial h_4}{\partial x} & 0 \\ 0 & 0 & \frac{\partial h_1}{\partial x} & 0 & 0 & \frac{\partial h_2}{\partial x} & 0 & 0 & \frac{\partial h_3}{\partial x} & 0 & 0 & \frac{\partial h_4}{\partial x} \end{bmatrix} \qquad (10)$$

The matrix $[B]$ for eight points can be written as follows:

$$[B] = \begin{bmatrix} \frac{\partial h_1}{\partial x} & 0 & 0 & \frac{\partial h_2}{\partial x} & 0 & 0,,,,,,,0 & 0 & 0 \\ 0 & \frac{\partial h_1}{\partial z} & 0 & 0 & \frac{\partial h_2}{\partial z} & 0,,,,,,,0 & \frac{\partial h_8}{\partial z} & 0 \\ 0 & 0 & \frac{\partial h_1}{\partial y} & 0 & 0 & \frac{\partial h_2}{\partial y},,,,0 & 0 & \frac{\partial h_8}{\partial y} \\ 0 & \frac{\partial h_1}{\partial y} & \frac{\partial h_1}{\partial z} & 0 & \frac{\partial h_2}{\partial y} & \frac{\partial h_2}{\partial z},,,,0 & \frac{\partial h_8}{\partial y} & \frac{\partial h_8}{\partial z} \\ \frac{\partial h_1}{\partial z} & \frac{\partial h_1}{\partial x} & 0 & \frac{\partial h_2}{\partial z} & \frac{\partial h_2}{\partial x} & 0,,,,,,,0 & \frac{\partial h_8}{\partial y} & \frac{\partial h_8}{\partial z} \\ \frac{\partial h_1}{\partial y} & 0 & \frac{\partial h_1}{\partial x} & \frac{\partial h_2}{\partial y} & 0 & \frac{\partial h_2}{\partial x},,,,\frac{\partial h_8}{\partial y} & ..0 & \frac{\partial h_8}{\partial x} \end{bmatrix} \qquad (11)$$

If we write this down for all 20 points, the matrix elements will be as follows**:**

$$[B]=\begin{bmatrix} \frac{\partial h_1}{\partial x} & 0 & 0 & \frac{\partial h_2}{\partial x} & 0 & 0 & \cdot & \cdot & \cdot & \frac{\partial h_{20}}{\partial x} & 0 & 0 \\ 0 & \frac{\partial h_1}{\partial z} & 0 & 0 & \frac{\partial h_2}{\partial z} & 0 & \cdot & \cdot & & 0 & \frac{\partial h_{20}}{\partial z} & 0 \\ 0 & 0 & \frac{\partial h_1}{\partial y} & 0 & 0 & \frac{\partial h_2}{\partial y} & \cdot & \cdot & & 0 & 0 & \frac{\partial h_{20}}{\partial y} \\ 0 & \frac{\partial h_1}{\partial y} & \frac{\partial h_1}{\partial z} & 0 & \frac{\partial h_2}{\partial y} & \frac{\partial h_2}{\partial z} & \cdot & \cdot & & 0 & \frac{\partial h_{20}}{\partial y} & \frac{\partial h_{20}}{\partial z} \\ \frac{\partial h_1}{\partial z} & \frac{\partial h_1}{\partial x} & 0 & \frac{\partial h_2}{\partial z} & \frac{\partial h_2}{\partial x} & 0 & \cdot & \cdot & & 0 & \frac{\partial h_{20}}{\partial y} & \frac{\partial h_{20}}{\partial z} \\ \frac{\partial h_1}{\partial y} & 0 & \frac{\partial h_1}{\partial x} & \frac{\partial h_2}{\partial y} & 0 & \frac{\partial h_2}{\partial x} & \cdot & \cdot & & \frac{\partial h_{20}}{\partial y} & 0 & \frac{\partial h_{20}}{\partial x} \end{bmatrix} \tag{12}$$

III.IVAnalysis of elasticity matrix components

Let us define a matrix for transversely isotropic masses in the half-space. The matrix dimensionis equal to $D(6x6)$. For inclined workings in the inclined transversely isotropic mass, the $d_{ij}^{'}$ elements are calculated using the formulas

$$\sigma_x+\sigma_y=9.5+2.98\gamma H,$$
$$\sigma_x=5+1.86\gamma H,$$
$$\sigma_y=4.5+1.12\gamma H, \tag{13}$$

$$\sigma_x+\sigma_y=5+2.14\gamma H,$$
$$\sigma_x=3+1.14\gamma H,$$
$$\sigma_y=2+\gamma H, \tag{14}$$

For (13) and (14), the general view of the elasticity matrix is set in the following way:

$$[D]=\begin{bmatrix} d_{11}^{'} & d_{12}^{'} & d_{13}^{'} & d_{14}^{'} & d_{15}^{'} & d_{16}^{'} \\ & d_{22}^{'} & d_{23}^{'} & d_{24}^{'} & d_{25}^{'} & d_{26}^{'} \\ & & d_{33}^{'} & d_{34}^{'} & d_{35}^{'} & d_{36}^{'} \\ & & & d_{44}^{'} & d_{45}^{'} & d_{46}^{'} \\ & d_{ij}^{'}=d_{ji}^{'} & & & d_{55}^{'} & d_{56}^{'} \\ & & & & & d_{66}^{'} \end{bmatrix}. \tag{15}$$

If we take that $\chi=0$ from expression $d_{ij}^{'}(E_1,E_2,G_2,\nu_1,\nu_2,\varphi,\psi,\chi,\ i,j=1,2...6)$ or from equation (14), we obtain the elements of the elasticity matrix for the *cross-drift* and *cut-off*. If we take that $\psi=\chi=0$ from equation (14), we get the elasticity matrix for the *boarding gate* in any inclined transversely isotropic mass. If $\varphi=\psi=\chi=0$ and $E_1=E_2, \nu_1=\nu_2,\ G_2=E_1/2(1-\nu_1)$, then we obtain the elasticity matrix for investigating the working's stability in the isotropic spatial mass. For the generalized plane problem, the elasticity matrix dimension equals $D(5x5)$, whereas for the plane problem this would be $D(3x3)$.

III.IV.I Determination of the stiffness matrix of the system $[K]$

When using a quadrangular, hexahedral element or an element in the form of a second-order prism, the stiffness matrix of each element is made by one of the following expressions:

$$u=\sum_{i=1}^{4}u_ih_i \qquad \vartheta=\sum_{i=1}^{4}\vartheta_ih_i \tag{16}$$

$$w=\sum_{i=1}^{4}w_ih_i$$

$$[J]^{-1}=\frac{1}{\det[J]}\begin{bmatrix} \bar{a}_{11} & \bar{a}_{12} & \bar{a}_{13} \\ \bar{a}_{21} & \bar{a}_{22} & \bar{a}_{23} \\ \bar{a}_{31} & \bar{a}_{32} & \bar{a}_{33} \end{bmatrix} \tag{17}$$

$$dV=dx\cdot dy\cdot dz=\det[J]\cdot d\xi\cdot d\eta\cdot d\zeta \tag{18}$$

The stiffness matrix $[K]$ of the entire computational region consists of the sum of the stiffness matrices of elements at points with single apexes. When using isoperimetric elements, the stiffness matrices of each element are composed of the values of the internal integration points and summed.

$$[K]=\sum_{e=1}^{p}[k]^e, \tag{19}$$

here p is the total number of finite elements in the research area.

III.IV.II Determination of geostatic force parameters γH

To determine the value of geostatic forces from the right side of equation (20), we multiply the specific weight of the structure γ by the area size when it is a quadrangular element or by the volume when it is an element in the form of a hexahedra on or a second order prism.

$$\bar{a}_{11}=a_{22}a_{33}-a_{23}a_{32},$$
$$\bar{a}_{12}=-(a_{21}a_{33}-a_{23}a_{31}),$$

$$\bar{a}_{13} = a_{21}a_{32} - a_{22}a_{31},$$

$$\bar{a}_{21} = -(a_{12}a_{33} - a_{32}a_{13}),$$

$$\bar{a}_{22} = a_{11}a_{33} - a_{31}a_{13},$$

$$\bar{a}_{23} = -(a_{11}a_{32} - a_{13}a_{12}),$$

$$\bar{a}_{31} = a_{12}a_{23} - a_{22}a_{13},$$

$$\bar{a}_{32} = -(a_{11}a_{23} - a_{21}a_{13}),$$

$$\bar{a}_{33} = a_{11}a_{22} - a_{12}a_{21}. \quad (20)$$

Then, by dividing by the number of vertices, we set these values to each point. At the common points, gravity forces are simply summed. Alternatively, we can multiply by the appropriate function-form of the element and assign to each point though Jacobian, while instead of H we use the Z coordinates for each point.

$$\gamma H_i = \gamma^e h_i z_i, \quad (21)$$

here i is the computational points on the vertices and sides of the element e. For an isotropic medium, horizontal components are equal to $\lambda\gamma H$. Here $\lambda = \frac{\nu}{1-\nu}$, ν is Poisson's ratio. In conditions of the plane problem for transversely isotropic masses, as defined by Yerzhanov, Aytaliyev, and Masanov, lateral thrust coefficients in two horizontal directions are different and equal [7]:

$$\lambda_x = \frac{(b_{13}b_{55} - b_{15}b_{35})(b_{11}b_{33} - b_{13}^2) - (b_{11}b_{35} - b_{13}b_{15})(b_{13}b_{35} - b_{15}b_{53})}{(b_{11}b_{33} - b_{13}^2)(b_{33}b_{55} - b_{35}^2) - (b_{13}b_{35} - b_{15}b_{33})^2},$$

,

$$\lambda_{xz} = \frac{(b_{33}b_{55} - b_{35}^2)(b_{11}b_{35} - b_{13}b_{15}) - (b_{13}b_{35} - b_{15}b_{33})^2}{(b_{11}d_{33} - b_{13}^2)(b_{33}b_{55} - d_{35}^2) - (b_{13}b_{35} - b_{15}b_{33})^2} \quad (22)$$

here b_{ij} is calculated by equation (4). Ifwe take the slope angle $\varphi = 0$ in this expression, we obtain the expression of Lekhnitskiy for planes of horizontally layered isotropy:

$$\lambda_x = \frac{\nu_2}{1-\nu_1}, \lambda_{xz} = 0, \quad (23)$$

here ν_1, ν_2 are Poisson's ratios for transversely isotropic masses.

III.IV.III Determination of tectonic forces T

The nature of tectonic forces has been studied by Aytmatov for the mines at Kadamzhai, Tekeli, and Haydarkent, which are located in the northern part of the Tien-Shan Mountains, where measurements have been made. On the basis of Hast's semi-empirical formulas, the following expressions have been proposed (24):

$$\sigma_x = b_{11}\varepsilon_x + b_{12}\varepsilon_y + b_{13}\varepsilon_z + b_{15}\gamma_{xz},$$

$$\sigma_y = b_{12}\varepsilon_x + b_{22}\varepsilon_y + b_{23}\varepsilon_z + b_{25}\gamma_{xz},$$

$$\sigma_z = b_{13}\varepsilon_x + b_{23}\varepsilon_y + b_{33}\varepsilon_z + b_{35}\gamma_{xz},$$

$$\tau_{yz} = b_{44}\gamma_{yz} + b_{46}\gamma_{xy},$$

$$\tau_{xz} = b_{15}\varepsilon_x + b_{25}\varepsilon_y + b_{35}\varepsilon_z + b_{55}\gamma_{xz}, \quad (24)$$

$$\tau_{xy} = b_{46}\gamma_{yz} + b_{66}\gamma_{xy}.$$

The same expressions were used by Turchaninov [13] who studied the influence of tectonic forces nan underground working in the isotropic mass; its values are shown in Fig. 10.

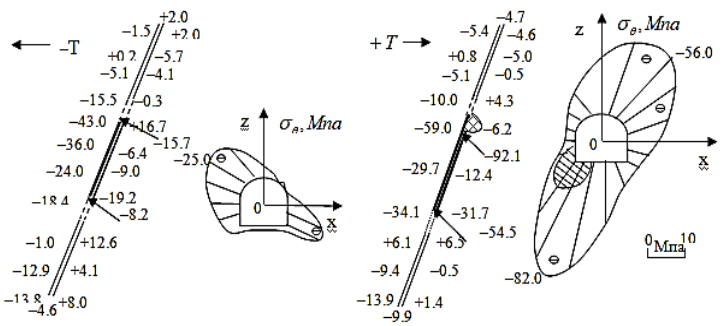

Fig. 10. The principal stress components of tectonic forces

Here we show the directions of tectonic forces that affect the elementary unit prism at any depth H from the Earth's surface.

Here T_H is the value of tectonic forces at depth H. Conventionally, its precise value is determined by measurements in vertical mines at various depths. Let us consider the anisotropic nature of tectonic forces from equation (8). First, $\sigma_3 = T_H$; T_H and σ_2 are defined through ψ_1 and ψ_2. According to the investigations of Kropotkin (1996) [14] and Turchaninov (1978) [13], among others, we obtain $\psi_1 \geq 0$ (i.e., the effect of this coefficient is quite insignificant) and $\nu \leq \psi_2 \leq 1$. For those are as not measured empirically, we can take $\psi_2 = 0.75$.

III.IV.IV The strength of relief roughness

Practically, this force again equals γH, but it is necessary to take into account the volume and weight of the slopes and mountains. When applying the FEM,for these to be taken into account, we only need to set the correct coordinates and further calculate this force by expression γH.

After determining the displacement vectors $\{U\}$ by solving the system of algebraic equations (9), stress components were determined using the following expressions:

$$J_{11} = \frac{1}{\det}\frac{\partial z}{\partial \eta},$$
$$J_{12} = \frac{1}{\det}\frac{\partial z}{\partial \xi},$$
$$J_{21} = \frac{1}{\det}\frac{\partial x}{\partial \eta},$$
$$J_{22} = \frac{1}{\det}\frac{\partial x}{\partial \xi}. \quad (25)$$

i.e.
$$[J]^{-1} = \frac{1}{\det}\begin{bmatrix} \frac{\partial z}{\partial \eta} & \frac{\partial z}{\partial \xi} \\ \frac{\partial x}{\partial \eta} & \frac{\partial x}{\partial \xi} \end{bmatrix}. \quad (26)$$

$$b_{1,1} = \sum_{mi=1}^{2} IJ_{1,m} P_{mi,1},$$

$$b_{21} = 0, \quad b_{31} = \sum_{mi=1}^{2} IJ_{2,m} P_{mi1},$$

$$b_{1,2} = 0, \; b_{22} = \sum_{mi=1}^{2} IJ_{2,m} P_{mi1,}$$

$$b_{32} = \sum_{mi=1}^{2} IJ_{2,m} P_{mi1,}$$

$$b_{1,3} = \sum_{mi=1}^{2} IJ_{1,m} P_{mi,2},$$

$$b_{23} = 0,$$

$$b_{33} = \sum_{mi=1}^{2} IJ_{2,m} P_{mi2},$$

$$b_{1,4} = 0,$$

$$b_{24} = \sum_{mi=1}^{2} IJ_{2,m} P_{mi2,}$$

$$b_{3,4} = \sum_{mi=1}^{2} IJ_{2,m} P_{mi2,}$$

$$b_{15} = \sum_{mi=1}^{2} IJ_{2,m} P_{mi3,}$$

$$b_{25} = 0,$$

$$b_{3,5} = \sum_{mi=1}^{2} IJ_{2,m} P_{mi3,} \quad (27)$$

$$b_{1,6} = 0,$$

$$b_{26} = \sum_{mi=1}^{2} IJ_{2,m} P_{mi3,}$$

$$b_{3,6} = \sum_{mi=1}^{2} IJ_{2,m} P_{mi3,}$$

$$b_{17} = \sum_{mi=1}^{2} IJ_{2,m} P_{mi4,}$$

$$b_{27} = 0,$$

$$b_{3,7} = \sum_{m=1}^{2} IJ_{2,m} P_{mi4},$$

$$b_{18} = 0,$$

$$b_{28} = \sum_{mi=1}^{2} IJ_{2,m} P_{mi4},$$

$$b_{3,8} = \sum_{mi=1}^{2} IJ_{2,m} P_{mi4,}$$

The values JJ can be written as follows[(25), (26), (27), (28) or (29), (30)]:

$$Det = J_{11} * J_{22} - J_{21} * J_{12} \quad (28)$$

$$a_{11} = \sum_{i=1}^{8} \frac{\partial h_i}{\partial \xi} x_i \qquad a_{12} = \sum_{i=1}^{8} \frac{\partial h_i}{\partial \xi} z_i \qquad a_{13} = \sum_{i=1}^{8} \frac{\partial h_i}{\partial \xi} y_i$$

$$a_{21} = \sum_{i=1}^{8} \frac{\partial h_i}{\partial \eta} x_i \qquad a_{22} = \sum_{i=1}^{8} \frac{\partial h_i}{\partial \eta} z_i \qquad a_{23} = \sum_{i=1}^{8} \frac{\partial h_i}{\partial \eta} y_i$$

$$a_{31} = \sum_{i=1}^{8} \frac{\partial h_i}{\partial \zeta} x_i \qquad a_{32} = \sum_{i=1}^{8} \frac{\partial h_i}{\partial \zeta} z_i \qquad a_{33} = \sum_{i=1}^{8} \frac{\partial h_i}{\partial \zeta} y_i. \quad (29)$$

$$[J] = \begin{bmatrix} a_{11} & a_{12} & a_{13} \\ a_{21} & a_{22} & a_{23} \\ a_{31} & a_{32} & a_{33} \end{bmatrix}. \quad (30)$$

Stress components are calculated through defined displacement components in the inner points of integration of each isoperimetric element, as follows:

$$\{\sigma_{ij}\} = [D]\{\varepsilon_{ij}\} \quad (31)$$

III.IV.V Physical-mechanical properties of transversely isotropic masses

Two modules ofelasticity, E_1, E_2, two Poisson's ratios, ν_1, ν_2, and a module of displacement, G_2, of transversely isotropic material in two perpendicular directions are defined byexperimental calculations. These values have not yet been entirely defined for all materials in nature.

Mountain layers on the seacoast in the town of Actau situated in the eastern part of the Caspian Sea in Kazakhstan are fully formed of sedimentary rocks. Their anisotropic properties were defined by Sivolapov [15]. We take the mean values for the mines given by Mikhlin [16] : $E_1 = 1.074 \cdot 10^4 MPa$, $E_2 = 0.523 \cdot 10^4 MPa$, $\nu_1 = 0.413$, $\nu_2 = 0.198$, $G_2 = 0.12 \cdot 10^4 MPa$, $\gamma = 2.5 \cdot 10^{-2} MN/m^3$.

III.IV.VI Physical-mechanical properties of isotropic masses

If the rock mass is isotropic, we take the following values for physical-mechanical properties: $E = 2 \cdot 10^4 MPa$, $\nu = 0.27$, $\gamma = 2.5 \cdot 10^{-2} MN/m^3$. As geologic faults in nature are filled with detrital and sedimentary rocks, their deformation values are high; therefore, for their characteristics, we use the following values: $E = 2 \cdot 10^2 MPa$, $\nu = 0.35$, $\gamma = 2.0 \cdot 10^{-2} MN/m^3$.

III.IV.VI Geometric dimensions of the computational region

The dimensions of the computational region, shown in Figs.3–8, were setusing the following conditions (9): $H = 600m$, $h = 300m$, $L = 1200m$, $H = 660m$, $h = 330m$, $L = 1500m$, $H = 660m$, $h = 330m$, $L = 1500m$. The height and length of the foundation of the arched working is 5 m, and the radius of the archis 2.5 m.

III. RESULTS AND DISCUSSION

Results of research addressing the mine working's stress state in the isotropic mass with complex tectonic faults are as follows.

We shall present the epures of stress concentrations and values in the vicinity of the geologic fissure and mine working for the plane problem, located in the isotropic mass at a distance of 5 m from the working shown in Fig.3.

Taking into account the fissure and working, the computational region is divided by 81 vertical and 51 horizontal lines, into 4000 four-vertex isoperimetric elements, conditionally forming 4131 points. The following values are taken for the length and width (2) of the computational region under the condition beginning from the mass's surface (the Earth's surface): $H = 600m$, $h = 300m, L = 1200m$. The physical-mechanical properties of the mass are left unchanged in Figs. 4–7. According to the regional condition (1), the horizontal displacement component is $U = 0$ in point 81 on the left side and point 81 on the right side of the region, shown in Fig.3, and $U = W = 0$ at the foundation. Considering the above, the order of the system of linear algebraic equilibrium equations made by expression (2) would be equal to 8000. The mass is supposed to be in an elastic state under the action of its gravity and the field of tectonic forces, the horizontal component of which is directed to the left. For the apexes of every element, the values of geostatic forces are given by expression (1) with an account of the lateral coefficient of compression. The composed system is solved by the algorithms (5)–(7). Deformation components in the internal points of integration are set by expression (25), and stress components have been calculated by expression (31).

The usage of a direct tangential component in the form of σ_θ for the analysis of stress concentrations at the boundaries of the mine working and fissure makes the task easier. Here θ is the polar angle between the perpendicular straight directions drawn to the boundaries of the working and the Cartesian horizontal OX axis. Let us present some known expressions from the elasticity theory of tangential components [17].

$$\sigma_r = \sigma_x \cos^2\theta + \sigma_y \sin^2\theta + 2\tau_{xz} \sin\theta \cos\theta,$$

$$\tau_{r\theta} = (\sigma_y - \sigma_x) \sin\theta \cos\theta + \tau_{xz} (\cos^2\theta - \sin^2\theta). \quad (32)$$

For analysis, it is more important to set displacement components in polar coordinates rather than deformation values.

If the value of stress concentrations on the ends of the working exceeds the breaking point of the rock, this place turns into plastic zone or a dangerous zone with the possibility of breaking. Such zones are defined by comparing the breaking point of the mass with stress intensity σ_i, which is the condition of transition of the border. Its expression in the spatial case is given below:

$$\sigma_i = \frac{1}{\sqrt{2}}\sqrt{(\sigma_x-\sigma_y)^2+(\sigma_y-\sigma_z)^2+(\sigma_z-\sigma_x)^2+6(\tau_{xy}^2+\tau_{yz}^2+\tau_{zx}^2)} \quad (33)$$

Table 1 provides data on the physical-mechanical properties and compression strengths of soils and mountain rocks at various depths h [18, 8].

Table 1. Physical-mechanical properties and compression strengths of soils and mountain rocks at various depths

Types	Soils and mountain rocks	h, km		$E\cdot10^{-4}$, MPa	ν	γ, 10^2 MH/m^3	σ_c, MPa	σ_p, MPa	τ_c, MPa
1	Bluestone	1.0		1.00	0.28	2.35	12.0	1.0	2.5
2	Clay, lime rock	1.0		1.23	0.25	2.35	14.5	1.0	2.5
3	Siltstone	0.6		2.0–4.0	0.27	2.43	60.0	3.0	6.0
4	Argillite	1.0		1.42	0.32	2.31	41.0	2.5	7.5
5	Quartz rock, pyrites	3.2		5.20	0.18	4.45	38.0	3.0	6.0
6	Crystalline limestone	2.8		2.10	0.27	3.06	47.0	3.0	8.0
7	Granitoid	4.0		10.60	0.28	2.87	46.5	7.0	11.0
8	Stone lime rock	6.0		83.00	0.24	2.50	285.0	12.5	60.0
9	Labradoritic basalt	10.0		141.00	0.25	3.40	396.0	16.5	66.0
10	Tholeiitic basalt	1.0		1.42	0.32	2.31	41.0	2.5	7.5
11	Picrite-basalt	1.0		1.35	0.31	2.43	24.0	3.0	6.0
12	Taxite basalt	1.0		1.82	0.26	2.33	32.5	1.5	6.0
13	Calcareous rock	1.0		1.23	0.25	2.35	14.5	1.0	2.5
14	Malmrock	3.2		1.00	0.27	2.35	12.0	1.0	2.5

Here σ_C is the vertical compression of the sample, σ_P is the vertical tension, and τ_c are the values received by experimental tangent compression. E, ν, γ are the Young's modulus, Poisson's ratio, and volumetric weight respectively.

Fig. 11 presents the epures of the vertical tangential component $\sigma_\theta / \gamma H$ calculated by expression (31), for stresses in the computational region shown in Fig.3.

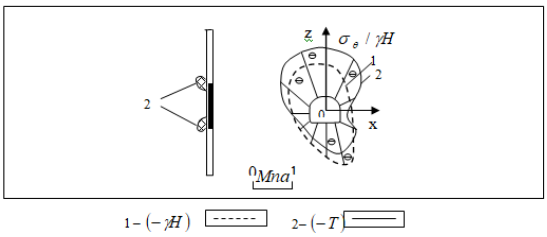

Fig. 11. The stress concentration on the ends of the mine working and around a fissure. (1) The effect of geostatic forces; and (2) the effect of tectonic forces

The physical-mechanical properties of the mass are close to siltstone, as described in Table 1. Here the displacement between the upper and lower fissures is 8 m. Consequently, the integrity of the mass around the working is left unbroken. The analysis of stresses is more optimally represented through portion γH, since the value of stress concentrations in distinction to γH is easier to be seen on the epures [19-25].

Based on the influence of geostatic forces alone, and considering tectonic forces ($-T$) directed to the left side of the plane in the vicinity of the working's arch, especially on the side directed to the fissure, the value ofthe tangential stress component increases by 20–25% and, as we move closer to the right side of the lower foundation, decreases. Potential breaking regions appear because stress concentrations exceed the mass's stability value on the ends of the upper and lower geologic fissures [26-31].

In Fig.12, the epures of stress concentrations in the vicinity of the fissures are shown on two sides of the mine working at a distance of 5 m, with one located higher and the other – lower. In this case, symmetry is not observed as tectonic forces are directed only to the left side.

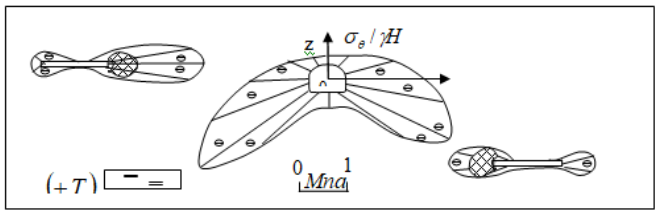

Fig. 12. The stress concentration on the ends of the mine working and in the vicinity of the direct fissures on either side of the working. (1) The effect of geostatic forces; and (2) the effect of tectonic forces

Fig. 13 and Fig. 14 show the stress epures occurring under the action of tectonic and geostatic stress fields.

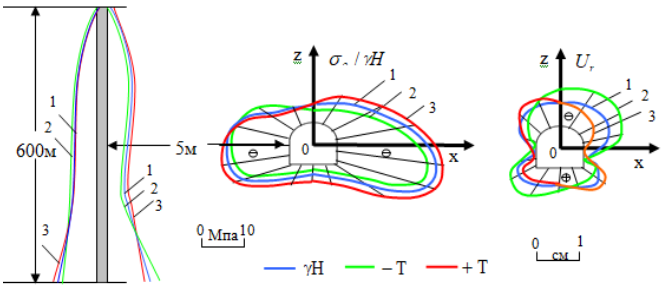

Fig. 13. The stress concentration on the ends of the mine working and in the vicinity of the direct fissures on either side of the working, under the action of geostatic forces

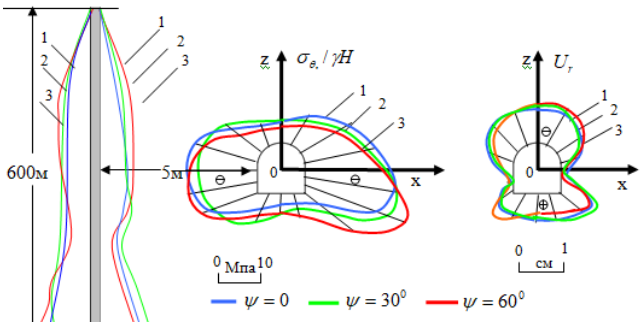

Fig. 14. The stress concentration on the ends of the mine working and in the vicinity of the direct fissures on either side of the working, under the action of tectonic forces

Fig. 15 and Fig. 16 show stresses in the vicinity of the horizontal fissures, appearing under the action of gravity and fields of tectonic forces, respectively. If tectonic forces act along with geostatic forces in the vicinity of the fissures located in the direction of mine workings, breaking is possible.

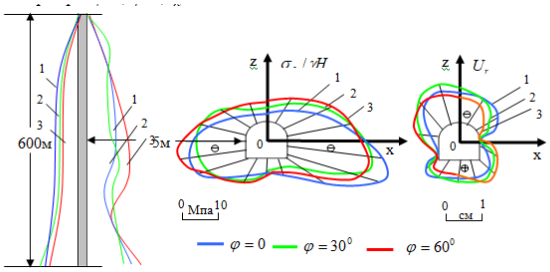

Fig. 15. The stress concentration occurring under the action of gravity in the mine working and an inclined fissure located at a distance of 15 m to the left. (1) Tectonic force directed to the left; (2) tectonic force directed to the right

As can be seen from Fig. 15, when no geologic fissure is found, the epure is symmetric. Its numerical value coincides with the above-calculated results of Baymakhan [8]. This comparison shows the correctness of the computational region and its calculating accuracy. In the presence of a geologic fissure, the value of stress concentrations on the left side of the mine working increases sharply and the epure'ssymmetry is broken. In this computational variant, the integrity of the mass in the vicinity of the mine working is preserved.

Fig.16 shows the effects of the direction of tectonic forces on stress concentrations. To more clearly understand these cases, in Fig.16, their directions are shown by arrows directed to the right and left. There are 14 m between the upper and lower fissures. In contradistinction to the epures given, Fig. 16 presents the exact values of stresses.

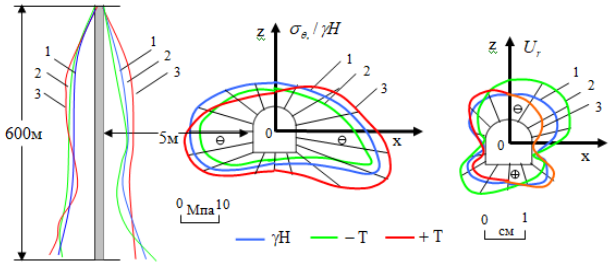

Fig. 16. The stress concentration occurring under the action of tectonic forces in the mine working and at the ends of an inclined fissure, located at a distance of 15 m to the left

Analyzing the epures of Fig.14, we can see that the epure of tectonic forces is represented by the first line directed to the left. The value of stresses is reduced with in the boundaries of the mine working and increased when approaching the fissure. In the lower part of the upper fissure, only at one point, the value of stability to compression is γH =2,5x300= 75 MPa, which is higher than the calculated stress value. If tectonic forces are directed to the right side, they will compress the mine working, and its value will increase sharply.

The numerical value of the epure will exceed the value of the mass's stability by approximately two-fold. Also, potential breaking zones may appear in the upper right corner of the mine working's arch and its lower left part. The form of the epure is

parallel to the inclined geologic fissure. The possible breaking zone appears in the lower part of the upper fissure and the upper part of the lower fissure in the left part of the mine working.

Fig.17 shows the stress states of the mine working in the vicinity of the geologic fissures, the ends of which are located in layers on the left and both sides of the working.

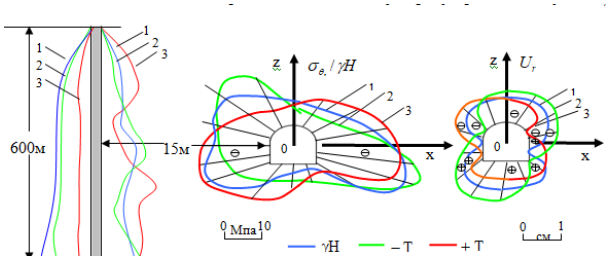

Fig. 17. The stress concentration occurring under the action of tectonic forces, directed to the right, in the mine working and various inclined fissures located to the left side of the working at a distance of 15 m. (1) Inclined and horizontally bifurcated fissures; (2) inclined fissures with embedded ends; (3) inclined fissures with embedded ends located in the upper and lower parts of the mine working

The strength of tectonic forces is directed to the right. From the analysis of these samples, we can see that the working is stable both on the screen of the bifurcated fissures and on the screen of two fissures located in layers. In the third case, if one of the geologic fissures ends in the upper left part of the mine working and the other fissure ends in the lower right part of the mine working, the stress concentration increases sharply and breaking becomes possible both on the working's arch and at its foundation. The same case is noted at the ends of the fissures.

IV. CONCLUSIONS

Here, using deformable solid mechanics methods, we investigated the stability of mine workings in a broken geologic mass under the action of tectonic forces. In recent years, multiple reviews have addressed urgent problems associated with the theory of underground structures, their mechanic-mathematical models, analytical and numerical techniques. New computational methods have been proposed based on the numerical method of stability in cases of underground workings in the mass, the integrity of which is subjected to geologic breaking. New criteria have been proposed for determining the finite element field of the working's stability in the half-space.

Also, using FEMs, new computational types of hexahedral elements for spatial modeling of the transversely isotropic area, including geologic fissures and underground workings, together with their complete algorithms, have been developed.

If the mine working, under the effect of geologic fissures is also affected by geostatic and tectonic forces, the stress concentration in the transversely isotropic mass is generally gathered in the vicinity of two lateral sides of the mine working under the condition that the epures of the vertical tangential stress component in the isotropic massare directed along the length of the fissure or close to it.

In anisotropic medium, stress concentrations at the ends of the mine working, located under the inclined fissure, are much larger than under the vertical fissure.

In contradistinction to mine workings located near vertical and horizontal fissures, potential breaking regions appear on the corners of the working's foundations located closer to the inclined fissures.

For the mine workings of transversely isotropic masses, a larger stress concentration was detected on the sides, located closer to the fissure. The epures on the side of the geologic fissure, located closer to the mine working, are subjected to more significant changes. The father the fissure is located from the mine working, the lesser the concentration of stresses that accumulate in their walls. The various inclinations of the isotropic planes of the transversely isotropic mass affect the values and forms of stress concentrations. The epures of displacement components are subjected to changes along their vertical axis, in which the vicinity of the arch is compressed, and the vicinity of the foundation is stretched. The working does not affect the value of stresses on the left side of the fissure located closer to it.

We also found that the mountain's height affects the stress concentration at the ends of the working, located at a depth of 300 m to the left. When passing through the transverse geologic fissure occurring in the transversely isotropic mass in the direction of the mine working's digging, the stress concentration increases sharply in the vicinity of the fissure's walls.

Thus, here we propose a novel approach for addressing the mine working's stability in the broken anisotropic mass in the half-space. Optimal algorithms associated with this approach are presented, and the method has been validated using test cases. We established the design parameters for anisotropic and isotropic masses in the vicinity of the mine working and investigated the stress-deformed state of the mine working, first for an isotropic mass and then for an inclined transversely isotropic mass(plane deformation and spatial cases).We also presented a number of epures and analyzed the main computational results, namely the stress concentration and the radial displacement component on the lateral sides of mine workings and geologic fissures.

As a result of this research work, the following patterns were determined for calculating the stress concentration around an underground mine:

1. The greatest concentration of stresses near the mining output accumulates near the geological fault, the values and shapes of the stress concentrations are affected by the angle of inclination of the isotropy plane in the anisotropic massif.

2. The height of the mountain is directly proportional to the magnitude of stress concentration near the underground mine workings.

3. When a transverse geological crack occurs in a transversely isotropic mass in the direction of digging, the stress concentration increases sharply near the walls of the crack.

REFERENCES

[1] Dinnik A. N. Stability of elastic systems: textbook. benefits for high-boots. Moscow, Leningrad: ONTI NKTP USSR, 1935.

[2] Aytmatov IT, Erneev RY () Strategic issues of revival and development of coal mining in Kyrgyzstan. Mining Informational and Analytical Bulletin (scientific and technical journal). 2010; 1: 370-374.

[3] Ivanychev DA. The method of boundary states in problems of the elasticity theory for an anisotropic medium. Doctoral dissertation. Lipetzk, 2010.

[4] Hodzhiboyev AA. Solving the problems of structural mechanics with regard to anisotropy. Crack formation and heterogeneity of the medium on the basis of the development of the method of boundary equations. Author's summary of doctoral dissertation. Moscow, 2013.

[5] Fotiyeva NN, Bulychev NS, Firsanov ES, Deev PV. The bearing capacity of lining of parallel tunnels of an arbitrary cross-section. Moscow, Mountain Book. 2009; 3: 15-19.

[6] Aytaliyev SM, Baymakhanov IB, Masanov ZK, Fedotov SA. Method for assessing the impact of seismicity on the stability of Udokan copper mine. In: Problems of mining production in Eastern Siberia. Novosibirsk (pp. 10-17). Novosibirsk: Science. Siberian Branch, 1991.

[7] Masanov ZK. The spatial seismicity problem of underground structures in a folded mass. Author's summary of doctoral dissertation. Alma-Ata, 1991.

[8] Baimakhan AR, Baimakhan RB, Seinassinova AA, Kurmanbekkyzy N, Baimahanova GM. A calculation model for the landslide weak soil base of a tilted structure of buildings and constructions. International Journal of Civil Engineering and Technology (IJCIET). 2018; 9(11): 2859-2871.

[9] Aytmatov IT, Kozhagulov KC, Nikolskaya OV. Conceptual aspects of solving the problem of the stability of mountain roads in seismically active mountain-folded areas. Proceedings of the International Scientific Conference "Modern Conceptual Provisions in the Mechanics of Rocks". Bishkek, Ilim, 2002, pp. 166-169.

[10] Brinkgreve RBJ, Swolfs WM, Engin E, Waterman D, Chesaru A, Bonnier P, Galavi V. PLAXIS 2D Reference manual. Delft University of Technology and PLAXIS. The Netherlands, 2011.

[11] Zienkiewicz O, Morgan K. Finite elements and approximation. Moscow: Mir, 1986.

[12] Hageman LA, Young DM. Applied iterative methods. SIAM Review. 1986; 25(2): 281-283.

[13] Turchaninov IA. Tectonic stresses in the Earth's crust and stability of mine workings. Leningrad, 1978.

[14] Kropotkin PN. Tectonic stress in the Earth's crust. Geotectonics. 1996; 2: 3-15.

[15] Sivolapov KV. To the manifestation of creep of the rocks of the seabed under the weight of the oil and gas pipeline. Proceedings of the second international scientific and practical conference "Transport of Eurasia: A Look into the XXI Century". Almaty, 2002, pp. 245-247.

[16] Mikhlin S. Singular Integral Equations with Two Independent Variables. Mat. Sb. 1936; 1(43): 535-552.

[17] Terebushko OI. Fundamentals of the elasticity and plasticity theory. Moscow: Nauka, 1984.

[18] Handbook (CADASTRE) of physical properties of rocks. Moscow: Nedra, 1975.

[19] Arnold D, Demyanov V, Tatum D, Christie M, Rojas T, Geiger SP, Corbett P (2013) Hierarchical benchmark case study for history matching, uncertainty quantification and reservoir characterisation. Computers & Geosciences 50: 4–15

[20] Atymtayeva LB, Masanov JK, Myrzakhmetova GS, Iagalieva BE. Stationary diffraction of elastic waves on non-reinforced workings in an anisotropic layered mass. International conference "Modern problems of applied mathematics and mechanics: theory, experiment and practice." Dedicated to the 90th anniversary of the birth of Academician N. N. Ianenko. Novosibirsk, 2011, pp. 75-81.

[21] Harish, B. Application of block tectonic model and interblock tectonics at Koteshwar Dam Project. Proceedings of the conference on Recent Advances in Rock Engineering (RARE 2016). Series: Advances in Engineering Research, 2016.

[22] Bulychev NS. Mechanics of underground structures in examples and tasks. Moscow: Nedra, 1989.

[23] Durand-Riard P, Guzofski C, Caumon G, Titeux MO. Handling natural complexity in three-dimensional geomechanical restoration, with application to the recent evolution of the outer fold and thrust belt, deep-water Niger Delta. AAPG Bulletin. 2013 ; 97(1): 87-102.

[24] Laurent G, Caumon G, Bouziat A, Jessell M. A parametric method to model 3D displacements around faults with volumetric vector fields. Tectonophysics. 2013 ; 590: 83-93.

[25] Rysbayeva GP. Regularities of cracking on the contour of an underground structure in an anisotropic massif. Author's summary of doctoral dissertation, Al-Farabi Kazakh National University. Almaty, 2010.

[26] Segerlind L. Applied finite element analysis. New York: Wiley, 1976.

[27] Sekulovich M. The finite element method. Moscow: Stroyizdat, 1993.

[28] Seynasinova AA. The stress state of a loosely bound mass in the vicinity of underground excavation with regard to natural and artificial heterogeneities. Author's summary of doctoral dissertation, Al-Farabi Kazakh National University, Almaty, 2010.

[29] Wu Q, Xu H. 3D geological modeling and its application in Digital Mine. Science in China. 2014; 57(3): 491-502.

[30] Yeskaliyev MYe, Salgarayeva GI, Kurmanbekkyzy N, Katayev NS, Auelbaekov O. On the Definition of Limit Zones in the Layered Array with the Development of Various Flow Conditions. International Journal of Applied Engineering Research. 2016; 11(7): 5284-5287.

[31] Yudenkov AV, Adigamov AE, Izotova OA, Volodchenko AM. Mathematical models of problems of the theory of elasticity of an anisotropic body on the class of random functions. Mining Informational and Analytical Bulletin (scientific and technical journal). 2010; 1:75-80.